Detecting GPC3-Expressing Hepatocellular Carcinoma with L5 Peptide-Guided Pretargeting Approach: An *In Vitro* MRI Experiment

Weiyue Li[1,2], Xiang Xiao[1], Yikai Xu[1], Lichao Ma[1], Xiaodan Li[1], Liuji Guo[1], Chenggong Yan[1] and Yuankui Wu[1,*]

[1]*Department of Medical Imaging Center, Nanfang Hospital, Southern Medical University, Guangzhou, 510515, China*

[2]*Department of Radiology, Shenzhen People's Hospital, Shenzhen, 518020, China*

Abstract: *Background and Aim*: Glypican-3 (GPC3) is a novel molecular target for hepatocellular carcinoma (HCC). This study investigated the potential of an L5 peptide-guided pretargeting approach to identify GPC3-expressing HCC cells using ultra-small super-paramagnetic iron oxide (USPIO) as the MRI probe.

Methods: Immunofluorescence with carboxyfluorescein (FAM)-labeled L5 peptide was performed in $HepG_2$ and HL-7702 cells. Polyethylene glycol-modified ultrasmall superparamagnetic iron oxide (PEG-USPIO) and its conjugates with streptavidin (SA-PEG-USPIO) were synthesized, and hydrodynamic diameters, zeta potential, T_2 relaxivity, and cytotoxicity were measured. MR T_2-weighted imaging of $HepG_2$ was performed to observe signal changes in the pretargeting group, which was first incubated with biotinylated L5 peptide and then with SA-PEG-USPIO. Prussian blue staining of cells was used to assess iron deposition.

Results: Immunofluorescence assays showed high specificity of L5 peptide for GPC3. SA-PEG-USPIO nanoparticles had ≈36 nm hydrodynamic diameter, low toxicity, negative charge and high T2 relaxivity. MR imaging revealed that a significant negative enhancement was only observed in $HepG_2$ cells from the pretargeting group, which also showed significant iron deposition with Prussian blue staining.

Conclusion: MR imaging with USPIO as the probe has potential to identify GPC3-expressing HCC through L5 peptide-guided pretargeting approach.

Keywords: Hepatocellular carcinoma, magnetic resonance imaging, peptide ligand, iron oxide.

INTRODUCTION

Hepatocellular carcinoma (HCC) is one of the most common human malignancies that affect diverse populations worldwide [1]. Early diagnosis plays a vital role in the management and treatment of patients with HCC. As mainstay imaging modalities, conventional contrast-enhanced computed tomography (CT) and magnetic resonance (MR) imaging suffer from low sensitivity and specificity for small HCC, especially lesions smaller than a centimeter [2], leading to a possible delay in diagnosis. A variety of novel CT and MRI technologies have been explored, such as perfusion CT or MRI, diffusion-weighted MR imaging, and MR imaging with superparamagnetic iron oxide (SPIO), ultrasmall superparamagnetic iron oxide (USPIO), or hepatobiliary agents. While these methods offer an increase in our ability to detect HCC, there is still much room for improvement [3-6]. Two major factors that need to be addressed are the formidable reticulo-endothelial system of the liver that eliminates extraneous contrast agents, and tumor heterogeneity in terms of radiological features [2, 7].

Molecular MR imaging using magnetic nanoparticles (NPs) to specifically target tumor cells has been well documented as a good method to address issues with HCC diagnosis [8-10]. Glypican-3 (GPC3) may be the most promising among the specific molecular targets for HCC; it is highly expressed on most HCC cells while absent in normal liver parenchyma or benign liver lesions [11-12], and is more specific and sensitive than current biomarkers for small HCC, such as alpha-fetoprotein [12-15]. Sham *et al*. successfully identified HCC foci using ^{89}Zr coupled with an anti-GPC3 monoclonal antibody (aGPC3) as a PET probe [16], and MRI can be used to detect HCC of very small size with USPIO-aGPC3 as a molecular probe [12]. Monoclonal antibodies (moAb) are widely used as ligands in molecular imaging for their extraordinary targeting specificity and affinity for tumor biomarkers [17]. However, several inherent limitations of moAb, such as immunogenicity and high cost, severely hinder clinical translation of moAb-based approaches [18]. As an alternative to moAb, tumor homing peptides can be chosen as effective vectors to guide imaging probes to tumor cells [19-23]. Moreover, peptide ligands offer several advantages over moAbs, such as fast blood clearance and excellent tissue penetration, which may produce a higher tumor-to-

*Address correspondence to this author at the Department of Medical Imaging Center, Nanfang Hospital, Southern Medical University, Guangzhou, 510515, China; Tel: 86+ 61642086; Fax: 86+ 61642028; E-mail: ripleyor@126.com

Weiyue Li and Xiang Xiao have contributed equally to this work.

E-ISSN: 2308-6483/18

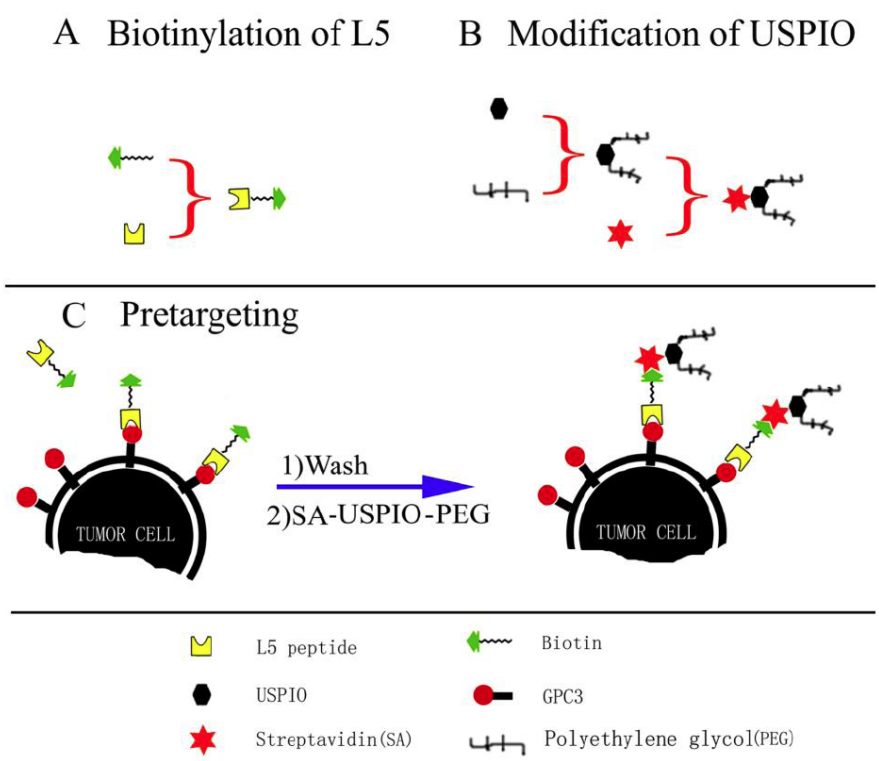

Figure 1: Schematic of the two-step pretargeting method using L5 peptide.

background ratio [24]. The L5 peptide consists of 14 amino acids (Arg-Leu-Asn-Val-Gly-Gly-Thr-Tyr-Phe-Leu-Thr-Thr-Arg-Gln) and targets GPC3-expressing HCC [23]. To the best of our knowledge, there is no published report on molecular MR imaging of HCC using L5 peptide targeting.

In this study, L5 peptide was utilized to bind GPC3 in HCC cells, and then biotinylation was employed to bridge superparamagnetic NPs with the L5 peptide through a two-step pretargeting protocol (Figure **1**). *In vitro* MR imaging and histologic examination were performed to evaluate the specificity and feasibility of the L5 peptide-based approach to identify GPC3-expressing HCC cells.

MATERIALS AND METHODS

Materials

L5 peptide (Arg-Leu-Asn-Val-Gly-Gly-Thr-Tyr-Phe-Leu-Thr-Thr-Arg-Gln) was purchased from Bambio Co, Ltd (Xiamen, China). FAM, 4′,6-diamidino-2-phenylindole (DAPI), 0.1M 2-morpholino-ethanesulfonic acid (MES) buffer solution, 1-ethyl-3-[3-dimethylaminopropyl] carbodiimide hydrochloride (EDC), sulfo-NHS, H_2N-PEG-COOH, MTT, Sulfo-NHS-LC-Biotin, and streptavidin (SA) were purchased from Sigma-Aldrich (St Louis, MO, USA). Dimethyl sulfoxide (DMSO), 4% paraformaldehyde, 2-mercaptoethanol, ethanolamine, and agarose were purchased from Aladdin-reagent (Shanghai, China). USPIO with carboxylate was purchased from Oneder Hightech Co. Ltd (Beijing China). All other chemicals were of analytical grade.

Cell Culture

$HepG_2$ and HL-7702 cell lines were gifts from the Research Center of Clinical Medicine in Nanfang Hospital (Guangdong province, China). Both cell lines were routinely grown in Dulbecco's modified Eagle's medium supplemented with 10% (v/v) fetal bovine serum and 1% streptomycin-penicillin in a humidified incubator at 37 ℃ with 5% CO_2.

Synthesis of L5-FAM

L5 peptide (1.0 mg/ml, 1.0 ml) was combined with 15 μg EDC and 20 μg of sulfo-NHS, and stirred for 20 minutes to activate the carboxyl group of the peptide. A desalting column was used to remove excessive EDC and sulfo-NHS, followed by the addition of 0.2 ml of FAM (1.0 mg/ml). The mixture was stirred at 4 ℃ in the dark for 12 hours. Excessive FAM was removed using the desalting column.

In Vitro Fluorescence Imaging

Fluorescence imaging was performed to verify the selective affinity of L5 peptide to GPC3-expressing

HCC cells. $HepG_2$ and HL-7702 cells were cultured on six-well chamber slides (5×10^5 per slide) and grown for 24 hrs at 37 ℃. Cells were washed with PBS three times, and fixed in 4% paraformaldehyde/PBS solution for 30 min. The fixative was then removed, and cells were washed again with PBS three times. The slides were incubated with 0.1mg/ml of L5-FAM or FAM in PBS/1% BSA, and then stained with DAPI for nuclear counterstaining. A blocking assay was conducted to evaluate L5 peptide specificity for GPC3, where the slides were incubated with 1mg/ml L5 peptide before adding 0.1mg/ml L5-FAM. Stained cells were observed with a fluorescence microscope (Eclipse TS100, Nikon).

Preparation of USPIO-PEG and SA-USPIO-PEG

A total of 10.0 mg of USPIO-COOH was dissolved in 10 mL MES buffer (pH 5.5). EDC (0.6 mg) and sulfo-NHS (0.4 mg) were added to the mixture to activate the carboxyl. After 20 minutes, a desalting column was used to remove excessive EDC and sulfo-NHS. H_2N-PEG-COOH (0.6 g) was added to the solution while stirring, and excessive PEG was removed. Then the PEG-USPIOs were concentrated by permanent magnet, and dissolved in MES buffer.

EDC (2.0 mg) and sulfo-NHS (5.5 mg) were added to PEG-USPIO in 0.1M MES buffer solution, and the reaction was maintained for 15 minutes at room temperature (RT) and then quenched with 2-mercaptoethanol. The solvent was removed by centrifugation at RT for 20 minutes at 2500 g (Millipore Amicon Ultra), the resultant NPs re-suspended in PBS buffer solution and mixed with SA (3.0 mg SA) for 2 hours while stirring at RT before the reaction was stopped by adding ethanolamine. Finally, the solution was ultrafiltered by centrifugation and the concentration was adjusted to 1.0 mg Fe/ml in PBS (pH 7.4).

NP Characterization

The surface charge and mean size distribution of PEG-USPIO and SA-USPIO-PEG in PBS were determined using Malven Zeta 3000HS (Malvern Instruments, Malvern, UK) operating at 633.0nm and 25.00 ± 0.05 ℃.

Magnetic Property Measurements

The T_2 relaxivity of PEG-USPIO and SA-USPIO-PEG was evaluated at 3.0T MR system (Signa Excite; General Electric, USA) using T_2 mapping sequence (TR=2000 ms, TE = 20, 40, 60, 80 ms, FOV=75×75 mm). Each NP was prepared in Fe concentrations of 0.04, 0.06, 0.08, 0.10, 0.12, 0.14, 0.16, 0.20, 0.40, and 0.60 mM. Images of the various solutions were analyzed by defining regions of interest (ROI) in each test tube. Relaxivity (R_2) value was calculated through the curve-fitting of T_2 (s^{-1}) vs. the Fe concentration (μM).

Cytotoxicity Assay

In vitro cytotoxicity of the NPs (PEG-USPIO and SA-USPIO-PEG) was evaluated using the MTT assay in HL-7702 cells. In short, HL-7702 cells were seeded in 96-well plates at 6×10^3 cells/well for 24 hours, and then incubated with PEG-USPIO or SA-USPIO-PEG at different concentrations (0.4, 0.8, 1.2, 1.6, 2.0 and 2.4 mM Fe) for 24 hours. Then, 20 μL of MTT (5.0 mg/mL) was added to each well and incubated for 4 hours, followed by the addition of 150 μL DMSO. The OD_{490} value of each well was measured using a BIOTEK ELX800 microplate reader. The control group only contained cells and culture medium.

Biotinylation of L5

L5 peptides were biotinylated with Sulfo-NHS-LC-Biotin following the manufacturer's protocol. After purification with an Amicon Ultra-15 Centrifugal Filter Unit with a 1 kDa membrane from EMD Millipore (Billerica, MA, USA), the final biotin-peptide ratio was approximately 4, as determined by the HABA method.

***In Vitro* MRI**

HepG2 and HL-7702 cells were seeded on 100 mm-diameter cell culture dishes and grown overnight. For the pretargeting group, 0.2 mg/ml of L5-BT was added to identify and bind to GPC3 molecules on tumor cells for 1 hour. Cells were then washed three times with PBS before the incubation with SA-USPIO-PEG (Fe concentration of 1.8 mM) for 2 hours. For the non-pretargeting group, cells were incubated with SA-USPIO-PEG at the Fe concentration of 1.8 mM for 2 hours. In the control group, cells were left untreated. All groups were detached using ethylene diamine tetra-acetic acid (EDTA) 1:5000 (Invitrogen), centrifuged, resuspended in 1% agarose at a concentration of 0.5×107 cells/ml, and then transferred into 1.5 ml centrifuge tubes. Six replicates for each group were performed. T2-weighted images were performed with SE sequence (TR=2500 ms, TE=96 ms, NEX=4, FOV=75×75 mm, thickness=2 mm, interval=2 mm). The T2WI signal intensity was normalized to that of 1%

agarose. T2 color maps of HepG2 and HL-7702 cells in 3 different groups were obtained.

Prussian Blue Staining

According to standard clinical pathology protocols, both $HepG_2$ and HL-7702 cells from the three groups (pretargeting, non-pretargeting and control) were stained with Prussian blue after MR imaging.

Statistical Analysis

All data are expressed as mean ± standard deviation. One-way analysis of variance and SNK were used to evaluate the differences of T_2WI signal intensity among three groups. All tests were performed using SPSS version 13.0 (IBM Corporation, Armonk, NY, USA). Results were considered statistically significant when $P<0.05$.

RESULTS

In Vitro Fluorescence Imaging

Cellular labeling with carboxyfluorescein (FAM) was visualized through fluorescence imaging. In the L5-FAM group, extensive cell membrane labeling occurred in $HepG_2$ (human hepatocellular carcinoma cells expressing GPC3) compared with HL-7702 (human normal hepatocytes not expressing GPC3) cells. In the FAM group, neither $HepG_2$ cells nor HL-7702 cells were labeled. In the blocking group, an excess of free L5 peptide precluded the binding of FAM-labeled L5 peptide to GPC3, resulting in a decreased fluorescent signal in $HepG_2$ cells (Figure **2**).

Characterization of PEG-USPIO and SA-USPIO-PEG

PEG-USPIO and SA-USPIO-PEG had an average hydrodynamic diameter of 22.73 nm and 35.97 nm, a polydispersity index of 0.207 and 0.169, and a zeta potential of 4.22 mV and -7.91 mV, respectively (Figure **3**).

Magnetic Property Measurements

The pseudocolored images of T_2 values illustrated that the color of the tubes deepened with an increase in Fe concentration (Figure **4**). R_2 values were 0.1394×10^3 $mM^{-1}s^{-1}$ and 0.1039×10^3 $mM^{-1}s^{-1}$ for PEG-USPIO and SA-USPIO-PEG, respectively (Figure **5**).

Cytotoxicity Assay

To evaluate the cytotoxicity of nanoparticles, HL-7702 cells were incubated with PEG-USPIO and SA-USPIO-PEG for 24 hours and then assessed cell viability via methyl thiazdyl tetrazolium (MTT) assay. As shown in Figure **6**, cell viability did not significantly change with increasing iron concentrations, and still remained above 80% at the maximal Fe concentration. These results demonstrated that both NPs display low toxicity and may be biocompatible at the given Fe concentration range (0.4-2.4 mM).

In Vitro MRI

In vitro MR imaging was performed to test the feasibility of identifying GPC3-expressing HCC cells through the L5 peptide-mediated pretargeting

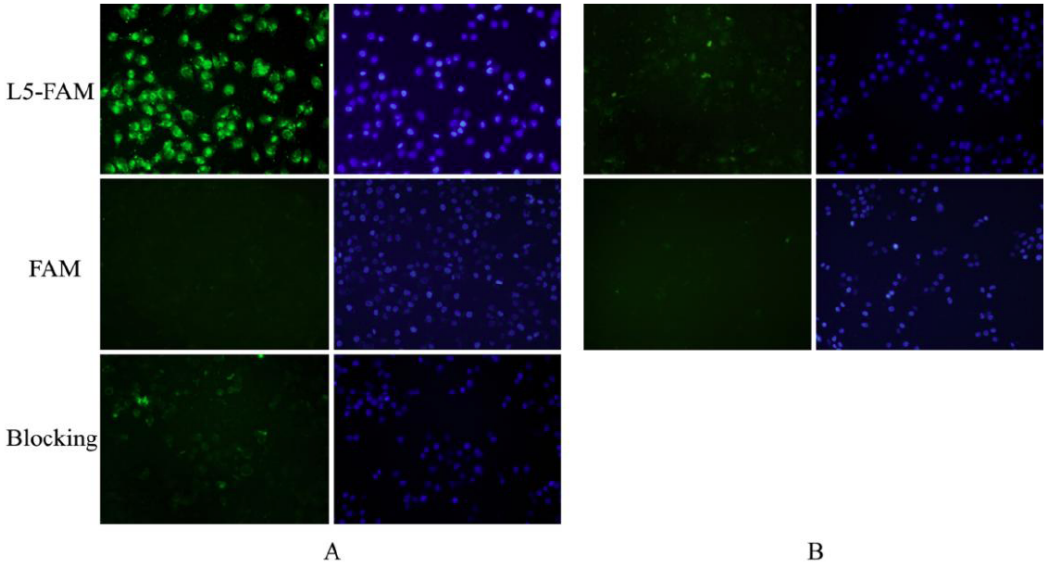

Figure 2: L5 peptide binding assays for (**A**) $HepG_2$ cells and (**B**) HL-7702 cells. Cells were incubated with either L5-FAM or FAM alone. Excess L5 protein was given to HepG2 cells with L5-FAM to exemplify competitive binding ("Blocking") and strong affinity of these compounds to GPC3.

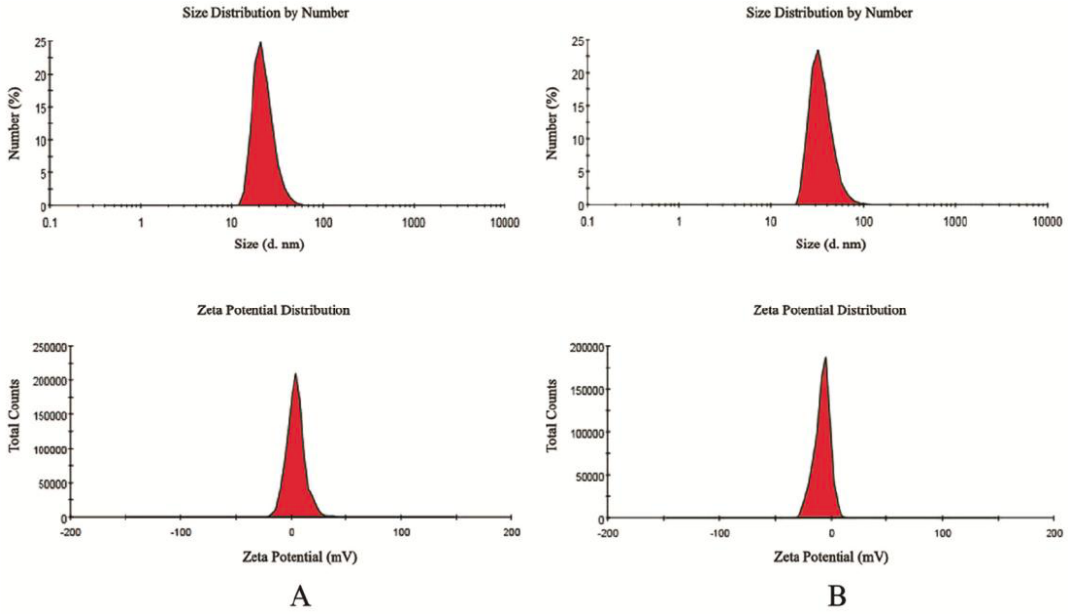

Figure 3: Dynamic light scattering data for (**A**) PEG-USPIO and (**B**) SA-USPIO-PEG.

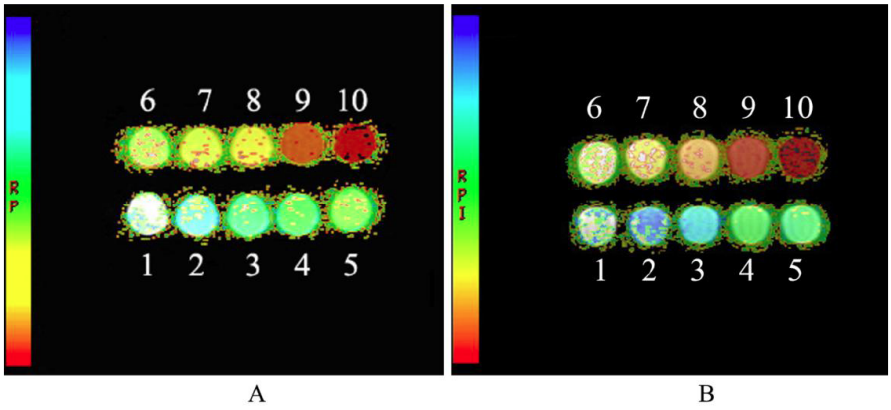

Figure 4: The T_2 color maps of (**A**) PEG-USPIO and (**B**) SA-USPIO-PEG. Numbers 1–10 represent Fe concentrations ranging from 0.04-0.6 mM.

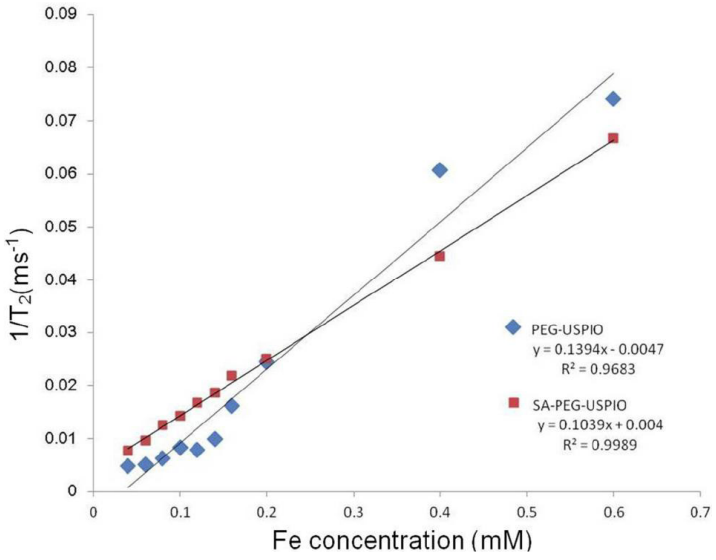

Figure 5: R_2 value curves of both NPs.

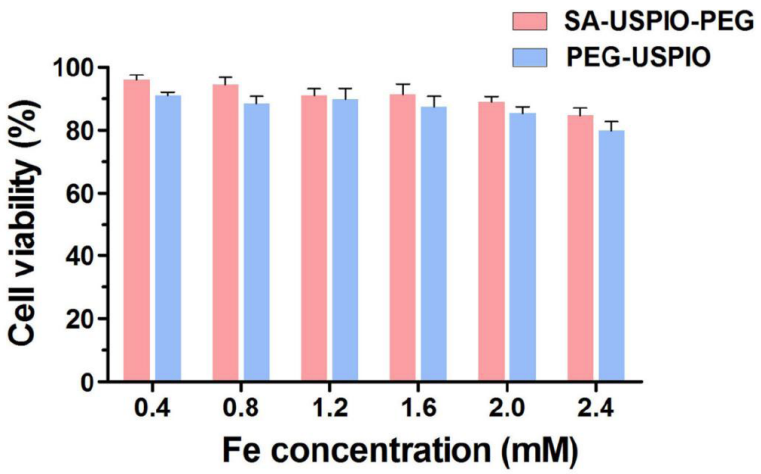

Figure 6: Cell viability of HL-7702 incubated with PEG-USPIO and SA-USPIO-PEG at various Fe concentrations.

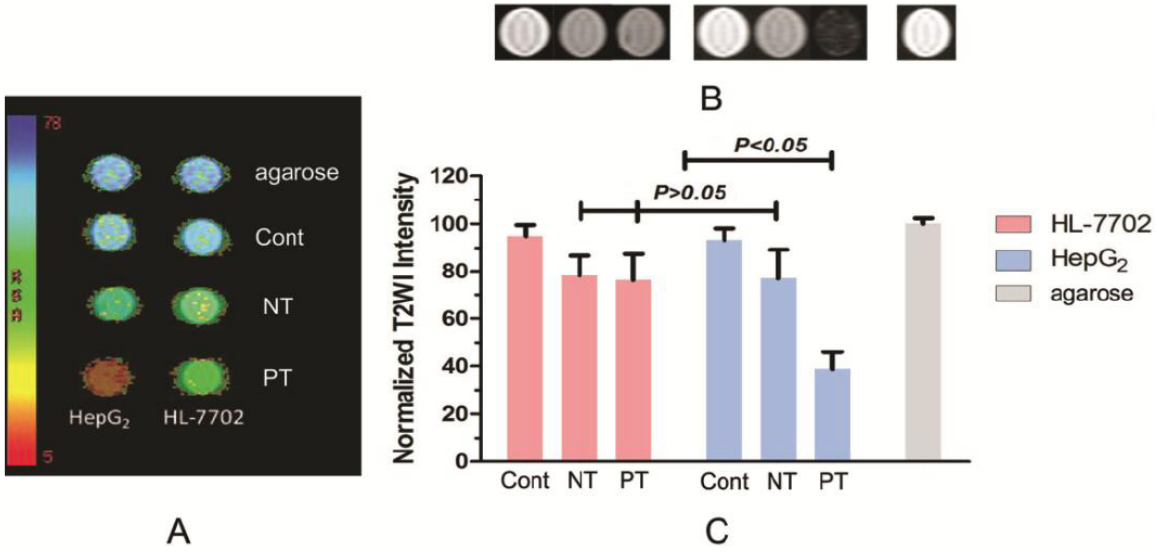

Figure 7: *In vitro* MR imaging of $HepG_2$ and HL-7702 cells in different treatment groups. (**A**) T_2 color maps, (**B**) T_2WI MR images, and (**C**) normalized T_2 signal intensities all demonstrate the most significant change in HepG2 cells in the pretargeting group. Abbreviations: Cont, control; NT, non-pretargeting; PT, pretargeting.

approach. Both the T_2 color maps and T_2WI images showed the most significant signal intensity decrease in $HepG_2$ cells in the pretargeting group (Figure **7A** and **7B**). A quantitative analysis showed that the normalized signal intensity of $HepG_2$ cells in the pretargeting group was lower than those of any other group (P<0.05), while the difference between the non-pretargeting and pretargeting groups in HL-7702 cells was not statistically significant (Figure **7C**).

Prussian Blue Staining

To evaluate the degree of NP uptake by tumor cells, Prussian blue staining was performed (Figure **8**). In the pretargeting group, numerous blue granules were found in most $HepG_2$ cells, in contrast to other groups with little to no blue granules.

DISCUSSION

In the present study, we demonstrated the potential of L5 peptide to serve as a specific ligand to guide magnetic NPs to GPC3-expressing HCC cells, as well as a way to intensify the signal, through a two-step pretargeting approach.

1. High Specific Ligand for GPC3

As an emerging molecular target for HCC, GPC3 has attracted increasing attention in the past decade [11, 15, 25, 26]. Anti-GPC3 moAb and its F(ab')2 fragment have proven to be effective tools in enabling tumor-specific diagnosis through their ability to deliver imaging probes directly to the GPC3 receptor [12,16, 26, 27]. Peptides have several advantages over moAb,

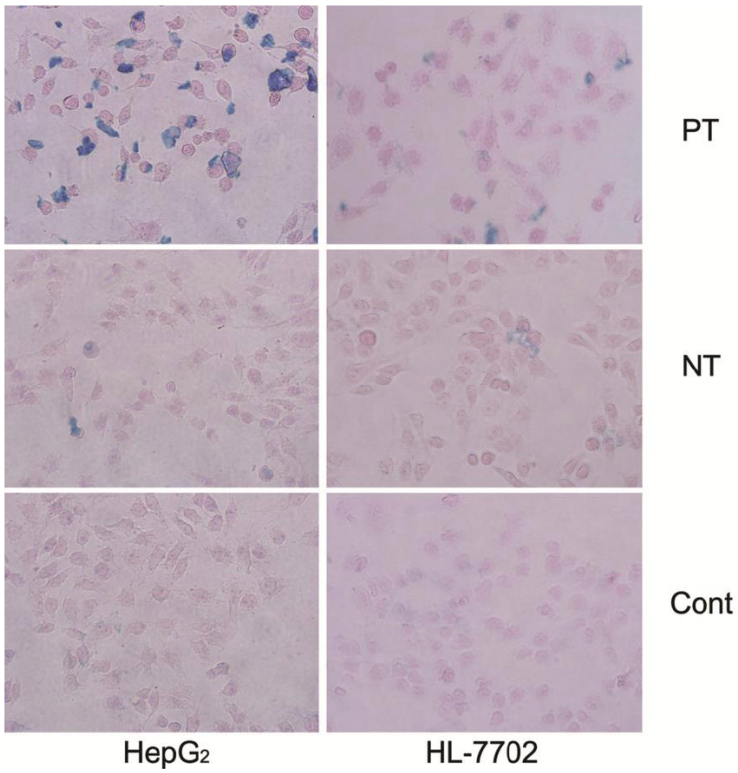

Figure 8: Prussian blue staining of $HepG_2$ and HL-7702 cells. Rich deposition of iron oxide particles (blue) is clear in the pretargeting group (PT) compared to non-pretargeting (NP) or control (Cont).

in that they are easy to synthesize and generally do not present with immunogenicity [18]. In a recent study by Lee's group, L5 peptide was shown to have strong affinity and high specificity for GPC3 [23]. In agreement with Lee's findings, direct immunofluorescence imaging and competitive binding assays in the present set of experiments demonstrated specific binding of L5 ligand to GPC3. Moreover, *in vitro* MRI showed a pronounced signal intensity decrease in the pretargeting $HepG_2$ group. The specificity of L5 peptide for GPC3 was further demonstrated by histologic examination. Of note, the signal intensities decreased approximately 20% in the HL-7702 groups (both pretargeting and non-pretargeting) and in the non-pretargeting $HepG_2$ group compared to control, which might be caused by a non-specific interaction between SA-USPIO-PEG particles and tumor or hepatic cells [26].

2. Modification of NPs

Iron oxide-based contrast agents are widely used in the field of molecular MR imaging because of their favorable properties such as superparamagnetism and safety [28]. Given the large amount of Kupffer cells in the liver capturing and eliminating extraneous particles, it is necessary to modify the surface of NPs to optimize the delivery efficiency of USPIO to their cellular targets [7]. Incorporation of PEG helps overcome biologic delivering barriers, increase access to targeted molecules and improve the biocompatibility of NPs [8, 29, 30]. In the present study, USPIO was coated with PEG and functionalized with SA; the resultant SA-USPIO-PEG maintained a high T_2 relaxivity, apart from showing low toxicity and a negative zeta potential. The negative surface charge allows deeper tissue penetration of SA-USPIO-PEG to the target by minimizing non-specific binding to surrounding tissues [31]. Also, the hydrodynamic size of nanoparticles is of importance, and is suggested to be controlled between 10 nm and 100 nm [8]. In the present study, the mean hydrodynamic size of SA-USPIO-PEG was about 36 nm. This would enable extravasation of the NP from leaky tumor vessels and accumulation in tumor cells via enhanced permeability and retention, while avoiding quick renal clearance [27, 32].

3. Biological Amplification for Molecular Imaging

One drawback to this general approach is that peptides have lower avidity to targeted molecules than do antibodies, owing to their smaller molecular sizes [17]. This would have a negative influence on the sensitivity of molecular imaging. The strategy based on the avidin–biotin system, either a two-step or three-step

protocol, is a versatile method to amplify signal intensity, and thus was employed in the present study to handle the potentially lower amount of NP uptake by tumor cells [33, 34]. In this preliminary study, we chose the less complicated two-step pretargeting protocol. The biotinylated L5 peptide was administered first to bind GPC3 on tumor cells (pretargeting), and then SA-NPs were administered to chase the biotinylated L5 peptide. Our results indicated that the two-step protocol is feasible with biotinylated L5 peptide as a reporter molecule for HepG2 cells, and USPIO-PEG as the contrast agent.

4. Limitations

While they were designed to serve as preliminary inquiries, several limitations of the present experiments should be noted, and are being further investigated. First, we have shown proof of principle in terms of cellular and molecular biology; however, whether or not this strategy will sufficiently aid with visualization of a GPC3-expressing tumor *in vivo* needs to be investigated. Second, the comparison between an anti-GPC3 monoclonal antibody and L5 peptide in terms of their efficacy to guide USPIO probes to tumor cells was not assessed. Further, since the pretargeting approach with avidin-biotin system is relatively complex, delivering magnetic NPs directly to HepG2 cells with a detectable L5 peptide, but without using the avidin-biotin system, is more desirable.

In summary, USPIO-based imaging probe with superparamagnetism and low cytotoxicity was synthesized, and the feasibility of the L5 peptide-mediated two-step pretargeting approach to specifically identify GPC3-expressing HCC was validated using *in vitro* MRI. This detection method may be useful in the early detection and diagnosis of HCC and other targetable cancers.

CONFLICTS OF INTEREST

The authors disclose no conflicts of interest.

GRANT SUPPORT

This research was supported by the Natural Science Foundation of Guangdong Province of China (No. S2013010015689), the Science and Technology Program of Guangzhou of China (No. 201707010003) and the Special Foundation of President of Nanfang Hospital, Southern Medical University of China (No. 2016B026).

REFERENCES

[1] Waller LP, Deshpande V, Pyrsopoulos N. Hepatocellular carcinoma: a comprehensive review. World J Hepatol 2015; 7(26): 2648-63. https://doi.org/10.4254/wjh.v7.i26.2648

[2] Choi BI, Lee JM. Advancement in HCC imaging: diagnosis, staging and treatment efficacy assessments: imaging diagnosis and staging of hepatocellular carcinoma. J Hepato-Bil-Pan Sci 2010; 17(4): 369-73. https://doi.org/10.1007/s00534-009-0227-y

[3] Youk JH, Lee JM, Kim CS. MRI for detection of hepatocellular carcinoma: comparison of mangafodipir trisodium and gadopentetate dimeglumine contrast agents. Am J Roentgenol 2004; 183(4): 1049-54. https://doi.org/10.2214/ajr.183.4.1831049

[4] Kim, YK, Kim CS, Kwak HS, Lee JM. Three-dimensional dynamic liver MR imaging using sensitivity encoding for detection of hepatocellular carcinomas: comparison with superparamagnetic iron oxide-enhanced MR imaging. J Magn Reson Imaging 2004; 20(5): 826-37. https://doi.org/10.1002/jmri.20188

[5] Gluskin JS, Chegai F, Monti S, Squillaci E, Mannelli L. Hepatocellular carcinoma and diffusion-weighted MRI: detection and evaluation of treatment response. J Cancer 2016; 7(11): 1565-70. https://doi.org/10.7150/jca.14582

[6] Kim SH, Kim SH, Lee J, Kim MJ, Jeon YH, Park Y, Choi D, Lee WJ, Lim HK. Gadoxetic acid-enhanced MRI versus triple-phase MDCT for the preoperative detection of hepatocellular carcinoma. Am J Roentgenol 2009; 192(6): 1675-81. https://doi.org/10.2214/AJR.08.1262

[7] Moghimi SM, Hunter AC, Murray JC. Long-circulating and target-specific nanoparticles: theory to practice. Pharmacol Rev 2001; 53(2): 283-318.

[8] Kievit FM, Zhang MQ. Cancer nanotheranostics: improving imaging and therapy by targeted delivery across biological barriers. Adv Mater 2011; 23(36): H217-47. https://doi.org/10.1002/adma.201102313

[9] Liu YJ, Chen ZJ, Liu CX, Yu DX, Lu ZJ, Zhang N. Gadolinium-loaded polymeric nanoparticles modified with Anti-VEGF as multifunctional MRI contrast agents for the diagnosis of liver cancer. Biomaterials 2011; 32(22): 5167-76. https://doi.org/10.1016/j.biomaterials.2011.03.077

[10] Huang KW, Chieh J J, Horng HE, Hong CY, Yang HC. Characteristics of magnetic labeling on liver tumors with anti-alpha-fetoprotein-mediated Fe3O4 magnetic nanoparticles. Int J Nanomed 2012; 7: 2987-96. https://doi.org/10.2147/ijn.s30061

[11] Ho M, Kim H. Glypican-3: a new target for cancer immunotherapy. Eur J Cancer 2011; 47(3): 333-8. https://doi.org/10.1016/j.ejca.2010.10.024

[12] Li YW, Chen ZG, Li F, Wang JC, Zhang ZM. Preparation and *in vitro* studies of MRI-specific superparamagnetic iron oxide antiGPC3 probe for hepatocellular carcinoma. Int J Nanomed 2012; 7: 4593-611. https://doi.org/10.2147/ijn.s32196

[13] Soresi M, Magliarisi C, Campagna P, Leto G, Bonfissuto G, Riili A, Carroccio A, Sesti R, Tripi S, Montalto G. Usefulness of alpha-fetoprotein in the diagnosis of hepatocellular carcinoma. Anticancer Res 2003; 23(2C): 1747-53.

[14] Ligato S, Mandich D, Cartun RW. Utility of glypican-3 in differentiating hepatocellular carcinoma from other primary and metastatic lesions in FNA of the liver: an immunocytochemical study. Modern Pathol 2008; 21(5): 626-31. https://doi.org/10.1038/modpathol.2008.26

[15] Kandil D, Leiman G, Allegretta M, Trotman W, Pantanowitz L, Goulart R, Evans M. Glypican-3 immunocytochemistry in liver fine-needle aspirates: a novel stain to assist in the differentiation of benign and malignant liver lesions. Cancer Cytopathol 2007; 111(5): 316-22. https://doi.org/10.1002/cncr.22954

[16] Sham JG, Kievit FM, Grierson JR, Miyaoka RS, Yeh MM, Zhang M, Yeung RS, Minoshima S, Park JO. Glypican-3-targeted 89Zr PET imaging of hepatocellular carcinoma. J Nucl Med 2014; 55(5): 799-804. https://doi.org/10.2967/jnumed.113.132118

[17] Yan YJ, Chen XY. Peptide heterodimers for molecular imaging. Amino Acids 2011; 41(5): 1081-92. https://doi.org/10.1007/s00726-010-0546-y

[18] McCarthy JR, Bhaumik J, Karver MR, Erdem SS, Weissleder R. Targeted nanoagents for the detection of cancers. Mol Oncol 2010; 4(6): 511-28. https://doi.org/10.1016/j.molonc.2010.08.003

[19] Arap W, Pasqualini R, Ruoslahti E. Cancer treatment by targeted drug delivery to tumor vasculature in a mouse model. Science. 1998; 279(5349): 377-80. https://doi.org/10.1126/science.279.5349.377

[20] Chaabane L, Tei L, Miragoli L, Lattuada L, von Wronski M, Uggeri F, Lorusso V, Aime S. *In vivo* MR imaging of fibrin in a Neuroblastoma tumor model by means of a targeting Gd-containing peptide. Mol Imaging Biol 2015; 17(6): 819-28. https://doi.org/10.1007/s11307-015-0846-4

[21] Hamilton AM, Aidoudi-Ahmed S, Sharma S, Kotamraju VR, Foster PJ, Sugahara KN, Ruoslahti E, Rutt BK. Nanoparticles coated with the tumor-penetrating peptide iRGD reduce experimental breast cancer metastasis in the brain. J Mol Med-Jmm 2015; 93(9): 991-1001. https://doi.org/10.1007/s00109-015-1279-x

[22] Wang QB, Li JF, An S, Chen Y, Jiang C, Wang XL. Magnetic resonance-guided regional gene delivery strategy using a tumor stroma-permeable nanocarrier for pancreatic cancer. Int J Nanomed 2015; 10: 4479-90. https://doi.org/10.2147/IJN.S84930

[23] La Lee Y, Ahn BC, Lee Y, Lee SW, Cho JY, Lee J. Targeting of hepatocellular carcinoma with glypican-3-targeting peptide ligand. J Pept Sci 2011; 17(11): 763-9. https://doi.org/10.1002/psc.1400

[24] Dijkgraaf I, Boerman OC, Oyen WJG, Corstens FHM, Gotthardt M. Development and application of peptide-based radiopharmaceuticals. Anti-Cancer Agent ME 2007; 7(5): 543-51. https://doi.org/10.2174/187152007781668733

[25] Kulik LM, Mulcahy MF, Omary RA, Salem R. Emerging approaches in hepatocellular carcinoma. J Clin Gastroentero 2007; 41(9): 839-54. https://doi.org/10.1097/MCG.0b013e318060ac52

[26] Sham JG, Kievit FM, Grierson JR, Chiarelli PA, Miyaoka RS, Zhang M, Yeung RS, Minoshima S, Park JO. Glypican-3-targeting F(ab')2 for 89Zr PET of hepatocellular carcinoma. J Nucl Med 2014; 55(12): 2032-7. https://doi.org/10.2967/jnumed.114.145102

[27] Park JO, Stephen Z, Sun C, Veiseh O, Kievit FM, Fang C, Leung M, Mok H, Zhang MQ. Glypican-3 targeting of liver cancer cells using multifunctional nanoparticles. Mol Imaging 2011; 10(1): 69-77. https://doi.org/10.2310/7290.2010.00048

[28] Kandasamy G, Maity D. Recent advances in superparamagnetic iron oxide nanoparticles (SPIONs) for *in vitro* and *in vivo* cancer nanotheranostics. Int J Pharm 2015; 496(2): 191-218. https://doi.org/10.1016/j.ijpharm.2015.10.058

[29] Kitagawa F, Kubota K, Sueyoshi K, Otsuka K. One-step preparation of amino-PEG modified poly(methyl methacrylate) microchips for electrophoretic separation of biomolecules. J Pharmaceut Biomed 2010; 53(5): 1272-7. https://doi.org/10.1016/j.jpba.2010.07.008

[30] Zou P, Yu Y, Wang YA, Zhong YQ, Welton A, Galbán C, Wang SM, Sun DX. Superparamagnetic iron oxide nanotheranostics for targeted cancer cell imaging and pH-dependent intracellular drug release. Mol Pharm 2010; 7(6): 1974-84. https://doi.org/10.1021/mp100273t

[31] Kim B, Han G, Toley BJ, Kim CK, Rotello VM, Forbes NS. Tuning payload delivery in tumour cylindroids using gold nanoparticles. Nat Nanotechnol 2010; 5(6): 465-72. https://doi.org/10.1038/nnano.2010.58

[32] Maeda, H. The enhanced permeability and retention (EPR) effect in tumor vasculature: the key role of tumor-selective macromolecular drug targeting. Adv Enzyme Regul 2001; 41: 189-207. https://doi.org/10.1016/S0065-2571(00)00013-3

[33] Yan CG, Wu YK, Feng J, Chen WF, Liu X, Hao P, Yang RM, Zhang J, Lin BQ, Xu YK, Liu RY. Anti-alphavbeta3 antibody guided three-step pretargeting approach using magnetoliposomes for molecular magnetic resonance imaging of breast cancer angiogenesis. Int J Nanomed 2013; 8: 245-55. https://doi.org/10.2147/ijn.s38678

[34] Sharkey RM, Cardillo TM, Rossi EA, Chang CH, Karacay H, McBride WJ, Hansen HJ, Horak ID, Goldenberg DM. Signal amplification in molecular imaging by pretargeting a multivalent, bispecific antibody. Nat Med 2005; 11(11): 1250-5. https://doi.org/10.1038/nm1322

Received on 21-04-2018 Accepted on 25-05-2018 Published on 02-08-2018

http://dx.doi.org/10.12970/2308-6483.2018.06.02